Pore-scale fluid dynamics resolved in pressure fluctuations at the Darcy scale

Catherine Spurin[1], Gareth G. Roberts[2], Conor P. B. O'Malley[2], Takeshi Kurotori[1,3], Samuel Krevor[2], Martin J. Blunt[2], and Hamdi Tchelepi[1]

[1]Department of Energy Science & Engineering, Stanford University
[2]Department of Earth Science & Engineering, Imperial College London
[3]Department of Chemical Engineering & Engineering, Imperial College London

Corresponding author: Catherine Spurin, `cspurin@stanford.edu`

Abstract

Complex flow dynamics have been observed, at the pore-scale, during multiphase through porous rocks. These dynamics are not captured in large scale models exploring the migration and trapping of subsurface fluids e.g., CO_2 or hydrogen. Due to limitations in imaging capabilities, these dynamics cannot be observed directly at the larger, Darcy scale. Instead, by using pressure data from pore-scale (mm-scale) and core-scale (cm-scale) experiments, we show that fluctuations in pressure measured at the core-scale reflect specific fluid displacement events taking place at the pore-scale. The spectral characteristics of the pressure data depends on the flow dynamics, size of the rock sample, and heterogeneity of pore space. While high resolution imaging of large samples would be useful in assessing flow dynamics across many of the scales of interest, such an approach is currently infeasible. We suggest an alternative, pragmatic, approach examining pressure data in the time-frequency domain using wavelet transformation.

Plain Language Summary

Complex fluid dynamics have been observed in small pores within rocks. These dynamics have not been accounted for in larger scale modelling efforts of CO_2 or hydrogen. Limitations in imaging prevent the direct observation of these dynamic at larger scales, creating uncertainty in how these dynamics manifest at larger scales. But by analyzing the pressure data, and fluctuations in pressure measurements, we can infer the small-scale dynamics without imaging. We apply our findings to larger samples and discover that the fluctuations are dependent on the type of flow dynamics occurring, sample size, and the composition of the sample. We present a practical approach for assessing the dynamics at the larger scale, where direct imaging is currently infeasible, by exploring the pressure data using a technique called continuous wavelet transformation.

1 Introduction

Fluid flow in the subsurface is a complex process, controlled by the interaction of multiple fluids with one another, and a heterogeneous pore space. It is central to the safe storage of CO_2 in the subsurface (Rubin & De Coninck, 2005; Bachu & Adams, 2003; Benson et al., 2012), and the storage and retrieval of hydrogen underground (Boon & Hajibeygi, 2022; Thiyagarajan et al., 2022), as examples. Depending on the flow rate, fluid viscosity, wettability of the fluids, and connectivity of the pore space, different flow mechanisms will prevail (Blunt, 2017; Lenormand et al., 1983; Avraam & Payatakes, 1995; Spurin et al., 2019a, 2019b; Rücker et al., 2015; Zou et al., 2018; Zhao et al., 2016). These processes span many orders of magnitudes for both timescales and length scales, from sub-second to hours (Berg et al., 2013; Schlüter et al., 2017; McClure et al., 2020), and sub-pore to multi-pore (Berg et al., 2013; Moebius & Or, 2014; Spurin et al., 2020). Fluid flow is also heavily controlled by the heterogeneity of the rock, which in itself ranges from nanometers to kilometers (Ringrose & Bentley, 2016; Jackson et al., 2018).

This complexity makes modelling the flow and trapping of fluids in the subsurface challenging, with uncertainty in which flow processes are important to characterise at different spatial scales. For example, at the scale of a reservoir, many attempts to predict CO_2 plume migration in the subsurface resulted with the CO_2 arriving earlier and spreading out further than expected (Dance et al., 2019; Hosseini et al., 2013; Daley et al., 2011; Ringrose et al., 2013). These analyses focused on characterising heterogeneity in continuum-scale properties, like capillary pressure and relative permeability (Jackson & Krevor, 2020). However, observations made at the pore-scale show dynamics that are not incorporated within the framework of continuum-scale flow properties, such as intermittent pathway flow and ganglion dynamics (Spurin et al., 2019a, 2019b; Rücker et al., 2015; Gao et al., 2020; Avraam & Payatakes, 1995). Traditional continuum-scale models relate flow rate linearly to an average pressure gradient across the system. They do

not account for any fluctuations in pressure, or a non-linear relationship between flow rate and pressure gradient, both of which have been observed experimentally, and attributed to non-linear flow dynamics (Blunt, 2017; Muskat, 1938; Zhang et al., 2021). These dynamics may play a role in large-scale flow properties, and will influence plume migration (Spurin et al., 2020; Juanes et al., 2010; Zhang et al., 2021).

Micro-computed tomography (Micro-CT) experiments provide pore-scale observations of fluid-fluid interfaces *in situ* at resolutions of a few microns. However, experimental limitations including temporal resolution, expense, and management of vast quantities of data produced, mean it is currently infeasible to observe fluid-fluid interfaces at the centimetre to metre scale (the core-scale). Instead, medical CT scanners are used to measure saturation distributions (Akin & Kovscek, 2003; Pini & Madonna, 2016; Krevor et al., 2012). If observations of flow from pore-scale experiments are representative of flow at larger scales they can, in principle, be used to understand results from core-scale experiments. However, it is unclear if information about flow dynamics is being lost due to the limited spatial and temporal scales of the pore-scale experiments, or if pore-scale dynamics differ when sample size is increased. For example, viscous and gravity forces may become more important at larger scales, even in capillary-dominated regimes.
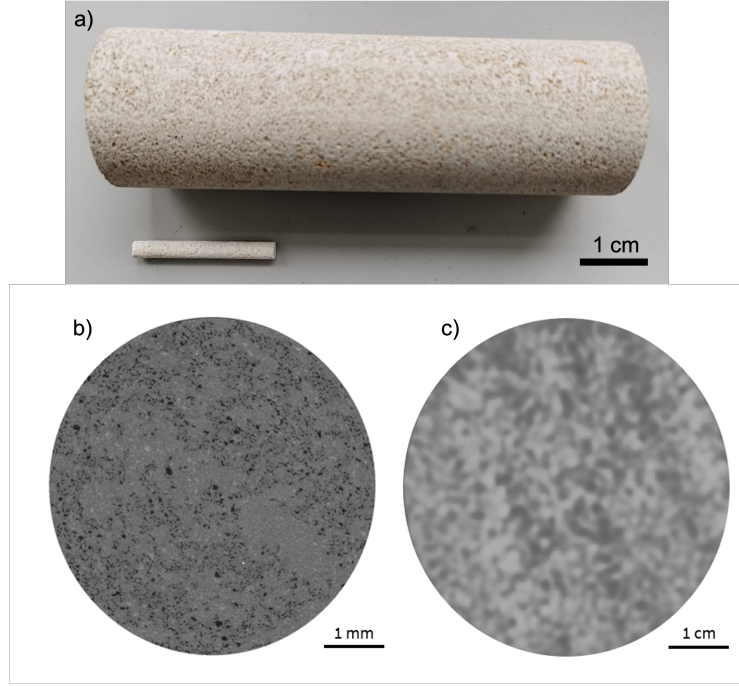
Pore-scale and core-scale experiments have two overlapping quantities that are measured: saturation and pressure. Saturation is important, as it can indicate the amount of trapping, but without a measure of connectivity, it gives no indication of the underlying dynamics. However, pressure fluctuations have been related to pore-scale dynamics and energy dissipation in the pore space through the creation and destruction of interfaces (Spurin et al., 2022; Rücker et al., 2021). In this work, we explore how pressure fluctuations measured during core-scale experiments can be used to provide insight into underlying flow dynamics by using continuous wavelet transforms to map the spectral power of pressure data. We identify sources of spectral power as a function of time and frequency. The merits of using pressure data to obtain information about multiphase flow in porous media, including possible scaling relationships, are assessed.

2 Methods

2.1 Experimental Procedure

The experiments in this work were conducted at two different scales: the pore-scale and the core-scale. For the pore-scale investigation, the sample was a carbonate rock, 5 mm in diameter and 20 mm long. These experiments were conducted at a synchrotron facility, so fluid interfaces could be resolved in real time (Spurin et al., 2020). There are two experiments in the pore-scale investigation, which both explored the transition to steady-state dynamics. One observes intermittent pathway flow through the co-injection of gas and water, while the other observes connected pathway flow through the co-injection of oil and water (Spurin et al., 2021, 2020). The capillary number, defined as $Ca = q/\sigma\lambda$ where q is the flow rate, σ is the interfacial tension and λ is the mobility of the fluids was 1.6×10^{-7} for the gas/water experiments and 2.2×10^{-6} for the oil/water experiments. See Spurin et al. (2020) for a full experimental description.

For the core-scale investigation, the sample was a carbonate rock, 5 cm in diameter and 12 cm long. The experiments were conducted in a medical CT scanner, so the fluid interfaces themselves cannot be resolved, but the saturation across many pores is measured (see Figure 1 for the difference in imaging resolution at the different scales). Three experiments were performed to explore the transition to steady-state dynamics; two explore the co-injection of gas and water. The same sample was used for both these experiments, but the sample orientation was reversed between experiments, to explore the role of heterogeneity of the pore space on flow dynamics. For the third experiment oil and water were co-injected. Sample orientation was not reversed in this experiment

Figure 1. (a) The core-scale (large) sample shown alongside the pore-scale sample to highlight the difference in scale. (b) A CT slice through the pore-scale sample, where fluid interfaces are resolvable. (c) A CT slice through the core-scale sample, where fluid interfaces are not resolvable but grayscale values are proportion to saturation.

as oil is difficult to remove from a sample, which would have influenced the observations. The capillary number was 2.0×10^{-8} for the gas/water experiments and 5.4×10^{-7} for the oil/water experiment. With similar capillary numbers, we aimed to observe the same manifestation of the pore-scale dynamics in the pressure data as the pore-scale experiments. The full experimental procedure is provided in the Supplementary Material.

An example of the images taken during an experiment at each scale is shown in Figure 1. It highlights the impact of the different imaging resolutions for the experiments, and shows how connectivity of the fluid phases cannot be calculated from traditional medical CT imaging. Thus, due to these imaging constraints, the only parameters that are constant across the experimental scales are saturation and pressure. The pressure drop across the the sample with time is the parameter of interest in this work, and was recorded for all experiments using a differential pressure transducer connected to the inlet line for the water, and the outlet line for both phases.

2.2 Spectral Analysis Using Wavelet Transformation

The spectral content of the pressure data was investigated by transforming it into the frequency-time domain using a continuous wavelet transformation (CWT). This differs from previous work using Fourier transformation of pressure data that revealed a cascade of timescales for steady-state multiphase flow, with lower frequency events having larger amplitudes (Spurin et al., 2022). While insightful, Fourier transforms have some limitations that make further analysis difficult. These include significant power spectral leakage, noisy calculated power spectra, and the fact that stationary functions are unlikely to reflect changes in pressure as a result of flow, especially during transient flow,

when average pressure is a function of time. Mapping spectral power as a function of frequency and time might provide additional insight into the dynamics of the system

We use a transform that convolves a uniformly-sampled pressure data time series, p_t, with a mother wavelet, ψ. Pressure time series, with constant sampling intervals of either $\delta_t = 1.29$ seconds (pore-scale experiments; Figure 2) or 9.3 seconds (core-scale experiments; Figures 3 & 4), were mirrored 7 times before being transformed to ameliorate edge effects (Roberts et al., 2019). The Derivative-of-Gaussian (DOG) wavelet, with derivative $m = 6$, was used as the mother wavelet in this study. It was scaled and translated along the time series by t' to reveal variations in amplitude as a function of scale, s, and time, t. Thus, the wavelet transform, $W_t(s)$, has the form:

$$W_t(s) = \sum_{t'=0}^{N-1} p_t \psi^* \left[\frac{(t' - t)\delta t}{s} \right] \tag{1}$$

where ψ^* denotes the complex conjugate of the mother wavelet. N is the number of discrete measurements of pressure. In this study, $N = 385$ for the gas/water core-scale experiments (total sampling duration ≈ 1 hour), for the oil/water core experiment $N = 577$ (≈ 1.5 hours). For the pore-scale experiments $N = 24,991$ (≈ 9 hours) and $14,081$ (≈ 4 hours) for gas/water and oil/water experiments, respectively. The code was adapted from O'Malley and Roberts (2022), and based on the methods summarized by Torrence and Compo (1998). The input signals can be recovered with errors less than 2.5% via the inverse transform, highlighting the fidelity of the transformations (see Supplementary Material).

The wavelet transform can be converted into power, ϕ, such that $\phi(t, s) = |W_t(s)|^2$. The time-averaged power spectrum is thus:

$$\phi(s) = \frac{1}{N} \sum_{t=0}^{N-1} |W_t(s)|^2. \tag{2}$$

Following (Liu et al., 2007), power is rectified by scale, and scales are converted into equivalent Fourier frequencies. The rectified time-averaged power spectra, $\phi_r = \phi(s)s^{-1}$, are consistent with results obtained from Fourier transformation of the time series.

Relationships between power spectral amplitudes and frequencies, f, provide insight into the scaling regimes and dynamics of many physical systems (Moura et al., 2017; Spurin et al., 2022; Rudnick & Davis, 2003; Fernandes et al., 2022; van der Schaaf et al., 2002). Many geophysical time series are characterised by:

$$\phi_r \propto f^\alpha. \tag{3}$$

Determining the value(s) of α from the power spectra of time series can be a convenient way to identify scaling regime(s). For example, $\alpha = -2$ indicates that a time series can be characterized as red noise. If pressure time series are characterized by red noise, it implies that the amplitudes of the pressure perturbations are proportional to their duration. White noise, $\alpha = 0$, indicates that the amplitudes of pressure perturbations are roughly the same across all frequencies. A variety of other noise distributions and changing patterns of spectral content can be straightforwardly identified by plotting power as a function of frequency in log-log space. For example, black, pink, and blue noise have spectral slopes, α, of -3, -1 and 1, respectively.

3 Results and Discussion

3.1 Sources of Spectral Power

There are many different potential sources for the spectral power in pressure time series during multiphase flow. The main ones identified here are (1) flow mechanisms (such as intermittent pathway flow or connected pathway flow), (2) heterogeneity of the pore space, and (3) the ratio of capillary to viscous forces.

In this research we focus on the flow mechanisms, and their representation in pressure signals in pore-scale experiments. This approach allows us to link spectral power to different flow regimes. We explore if the spectral scalings obtained can be applied to core-scale results to assess whether flow regimes can be deduced without pore-scale imaging. With the larger samples, we explore the role of heterogeneity on fluid flow by repeating the experiment with the sample orientation reversed, so that the direction of flow relative to the heterogeneity is reversed. Note that the degree and orientation of heterogeneity is linked to the flow mechanisms (Spurin et al., 2019a), so it is non-trivial to isolate them. With larger cores, viscous forces may also play a more important role.
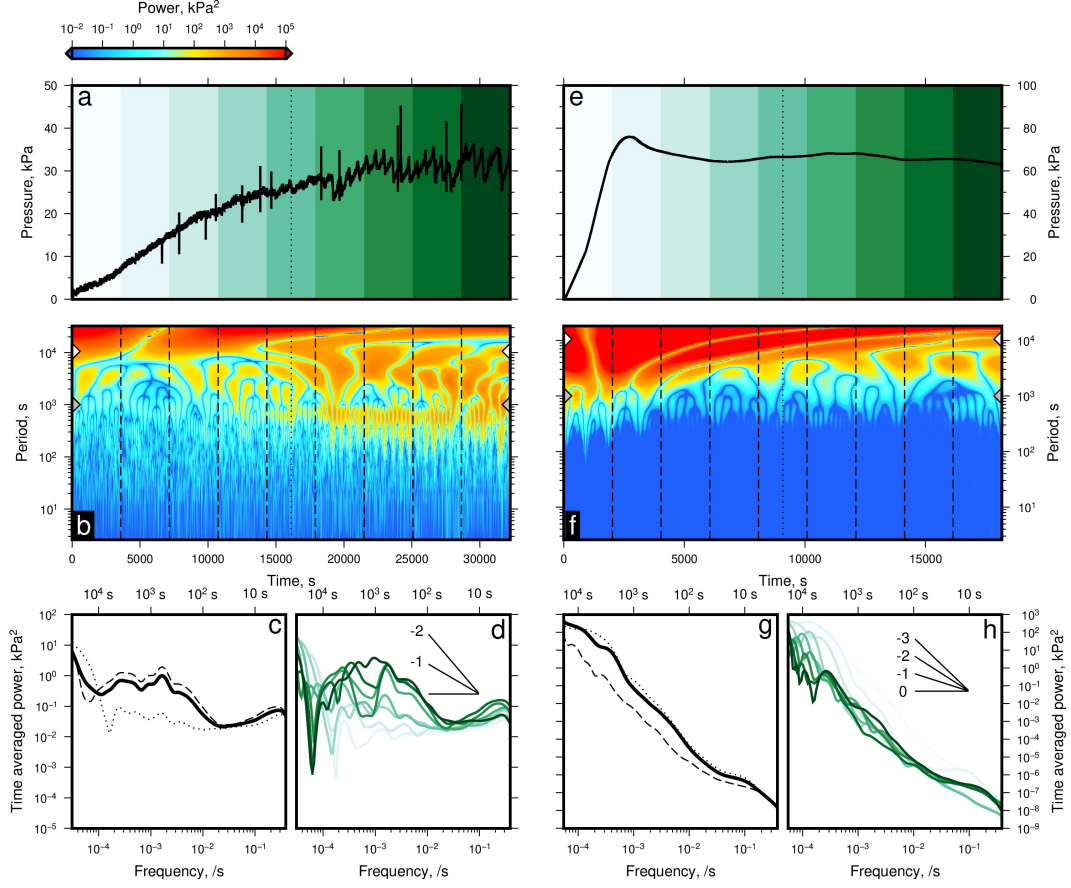
3.2 Pore-Scale Results

The results for the pore-scale experiments are shown in Figure 2, with panels a-d showing the results for the gas/water experiment and panels e-h showing the results for the oil/water experiment. Panels a and e in Figure 2 show the pressure drop across the sample recorded during an experiment for gas/water and oil/water, respectively. The shaded green strips correspond to the time intervals for the time-averaged power spectra shown in panels d and h, with a later time denoted by a darker shade. Note these panels indicate $\sim$ 1 hr intervals for the gas/water experiment, and $\sim$ 30 min intervals for the oil/water experiment because steady-state was reached quicker during the oil/water experiment. Figure 2b and f show power spectra of pressure data with time for gas/water and oil/water, respectively. Here, the dashed lines correspond to the shaded green strips in panels a and e. Figure 2c-d and g-h show time-averaged power against frequency for gas/water and oil/water, respectively. This is shown for the full recording window, and the 1$^{\text{st}}$ and 2$^{\text{nd}}$ half of the pressure time series in Figure 2c and g, which can be compared to the evolution of the power spectra for shorter intervals in Figure 2d and h.

With the pore-scale experiments, we can relate power spectra to different flow regimes observed during the experiments. For both experiments, the sample is initially saturated with water. First, the non-wetting phase (the gas or oil) percolates the sample, resulting in purely drainage events (gas or oil displacing the water). At approximately 20,000 s for the gas/water experiment (Figure 2a) and 3,000 s for the oil/water experiment (Figure 2e) the pressure plateaus, marking the transition to steady-state flow. For the gas/water experiment this leads to intermittent pathway flow, where gas flow pathways repeatedly connect and disconnect (Spurin et al., 2020). For the oil/water experiment no further displacement events occur during steady-state flow; the fluids flow in their own separate pathways that are connected across the pore space (Spurin et al., 2020).

3.2.1 Intermittent Pathway vs Connected Pathway Flow

For the gas/water experiment fluid rearrangement events were larger and occurred even during steady-state flow, while the oil/water experiment had little to no fluid rearrangement once oil had percolated the sample (Spurin et al., 2020, 2022). The different flow regimes are evident in the pressure in Figure 2a and e. First, in the oil/water experiment the pressure overshoots the stabilisation pressure (at around 3,000 s in Figure 2e), but then relaxes to approximately 65 kPa for the rest of the experiment. In the gas/water experiment, the pressure builds more gradually and then plateaus at approximately 20,000 s in Figure 2a. There are significantly more fluctuations during the gas/water

Figure 2. Spectral analysis of pressure time series from pore-scale experiments. (a) Black curve = pressure from gas/water experiment. Green strips and dotted line = time intervals indicated in panels b-d. (b) Power spectrum calculated by transforming black curve in panel a. Dashed and dotted lines correspond to time intervals indicated in panel a. Grey/white arrow heads indicate limit on low pass filters (10^3 and 10^4 s) discussed in body text. (c) Thick black curve = time-averaged, rectified, power spectrum for entire series. Dotted and dashed curves = time-averaged power for 1st and 2nd half of the time series, respectively (separated by dotted line in panels a and b). (d) Time-averaged power spectra for intervals indicated by green strips in panel a. Note graticule indicating red (-2), pink (-1) and white (0; flat) spectral slopes. (e-h) Results for the oil/water experiment.

experiment, even if the mean pressure remains constant, due to intermittent gas pathways periodically connecting and disconnecting.

Variations in the pressure time series are highlighted by the power spectra, produced by the continuous wavelet transformation, shown in Figure 2b and f. Several results are evident in the wavelet power spectra, which were not immediately obvious from inspection of the pressure time series alone. First, pressure at the longer periods/lower frequencies increases in power as the system transitions to steady-state for the experiment with intermittency (shown by the increase in power at periods of approximately 10^3 s in Figure 2b). This observation corresponds to the approximately 10 minute cycles observed in the pressure data in Figure 2a). These cycles were linked to disconnection and re-connection events in a key location, controlling flow across the sample (Spurin et al., 2020).

Secondly, pressure at shorter periods/higher frequencies contributes less to total power than the longer period fluctuations. Consider that inverse wavelet transforms produced including periods $> 10^3$ s have a mean error, which we define here as

$$\frac{1}{N\bar{p_t}} \sum_{t=1}^{N} \left[(p_t - p_{tf})^2 \right]^{1/2} \times 100(\%),\qquad(4)$$

where p_{tf} are pressures in the filtered series and $\bar{p}_t$ is mean pressure of the unfiltered series, of only 3% for the gas/water experiment (Figure 2b: grey arrow heads). The mean error is even less (2%) for the oil/water experiment (Figure 2f: grey arrow heads). Inverse transforms with only periods $> 10^4$ s included yield a mean error of 5% for the gas/water experiment, and 8% for the oil/water experiment (white arrow heads in Figure 2b and f, respectively). Shorter period variations in pressure ($< 10^3$ s), whilst still providing relatively little overall power, account for a greater proportion of the total power in the gas/water experiments compared to the oil/water experiment. In contrast, longer periods ($> 10^4$ s) contribute a relatively larger proportion of the total power for the oil/water experiment. In summary, pressure fluctuations at short periods play a greater role in larger scale flow properties in the gas/water experiment compared to in the oil/water experiment. This observation is indicative of the role that the pore-scale intermittency has in enabling flow at relatively little energy cost (Spurin et al., 2021).

Finally, time-averaged power spectra (Figure 2c-d and g-h) show that, for the gas/water experiment, different spectral slopes exist as the system evolves to steady-state conditions, transitioning from a slope of -1 (pink noise) to -2 (red noise) in Figure 2d, whilst a roughly constant spectral slope exists at all times and across all timescales during the oil/water experiment. This observation highlights the complexity of intermittent pathway flow, with events occurring over a wide range of frequencies, length-scales, and being non-local in nature (Spurin et al., 2020). At steady-state, intermittent pathway flow manifests as red noise (a spectral slope of -2) and connected pathway flow manifests as a spectral slope of -3. A slope of -2 agrees with observations made using Fourier transformation on steady-state pressure data (Spurin et al., 2022). A slope of -3 is typical for pseudo-turbulent flows (Mercado et al., 2010; Roghair et al., 2011; Mendez-Diaz et al., 2013). These are flows that appear turbulent but are in fact the result of the complex interaction of fluids with the surrounding space (other fluids, and in this case, potentially the rock grains) instead of inertial forces (Mercado et al., 2010). Further research, including velocity measurements are required to determine if pseudo-turbulence is occurring in multi-phase flow through porous media.

3.2.2 Possibility of Upscaling

For the oil/water experiment, where both fluids flowed in continuously connected pathways (as assumed in the multiphase extension of Darcy's law), a broadly constant
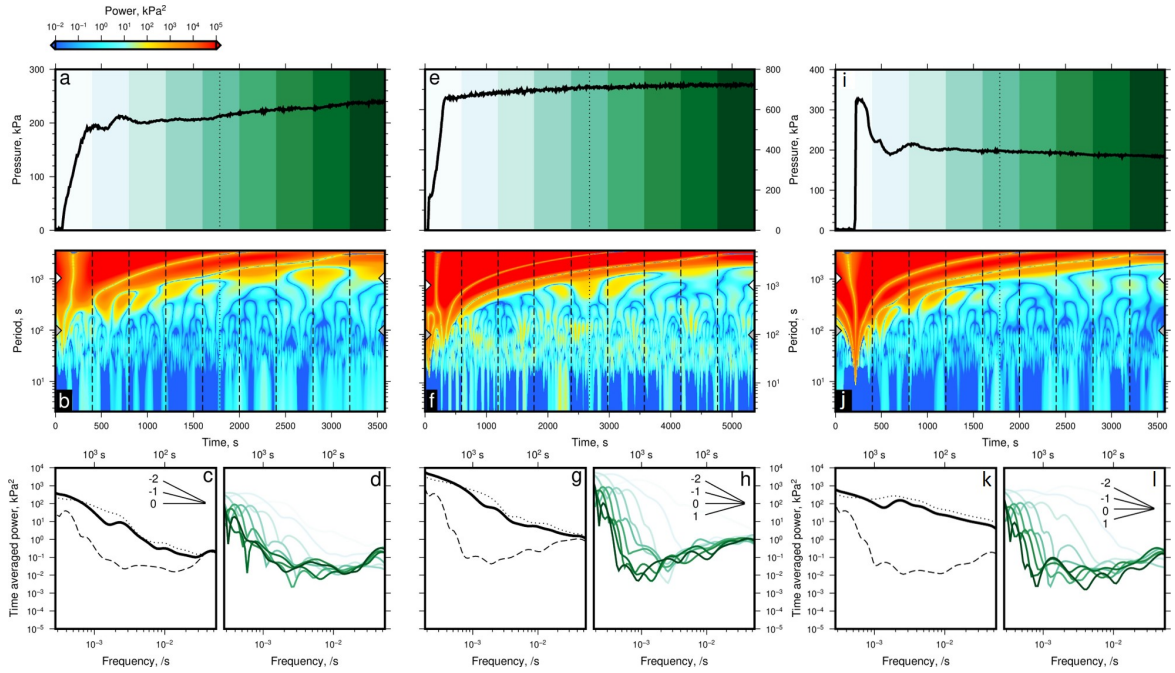
spectral slope of −3 exists for all frequencies during transient and steady-state flow (Figure 2h). These observations imply that there is limited temporal evolution during connected pathway flow, creating less uncertainty in predictions made for periods outside the experimental observation window.

For the gas/water experiment, spectral slopes depend on frequency and time, which implies a change in dynamics at different periods and times (Figure 2d). Spectral slopes steepen at long ($> 10^4$ s) and short ($< 10^3$ s) periods as the system transitions to 'steady-state' flow. This higlights the presence of non-linear dynamics not included in the multiphase extension of Darcy's law. The presence of multiple spectral slopes makes simple upscaling of predictions challenging. Thus, the success of upscaling efforts depends on how the dynamics present manifest in larger samples.

3.3 Core-Scale Results

The core-scale experiments follow the same procedure as the pore-scale experiments, with the same fluid pairings. This allows us to establish if the pore-scale observations can be upscaled to the core-scale experiments typically used for subsurface characterization (Pini & Benson, 2013; Perrin et al., 2009; Ruprecht et al., 2014). Figure 3a-d shows the results for the gas/water experiment, e-h shows the results for the oil/water experiment and i-l shows the results for the gas/water experiment in which sample orientation was reversed.

Figure 3. Spectral analysis of pressure time series from core-scale experiments. (a-d) Gas/water experiment initial sample orientation. (e-h) Oil/water experiment. (i-l) Gas/water experiment reversed sample orientation. Annotation is the same as Figure 2.

3.3.1 Gas/water vs Oil/water

The pressure response for the gas/water experiment and the oil/water experiment shown in Figure 3a and e appear similar in nature; in the first 500 s there is a steep increase in pressure as the gas or oil percolates the sample, then there is a gradual increase

in pressure with time, with pressure fluctuations of a similar magnitude (around 5 kPa). The spectral power provides additional insight into evolution of pressure, and reveals subtle differences between the experiments. First, power at longer periods ($> 10^3$ s) decreases with time, as shown by the reduction in red colours with increasing time in Figure 3b and f. Pressure at periods $> 10^3$ s contributes a similar proportion of power (mean error $\sim 2\%$) in both the gas/water and oil/water experiments (white arrow heads in Figure 3b and f). This implies that pressure at periods $> 10^3$ s contributes $\sim 98\%$ of total power.

Power at frequencies of 3×10^{-2} to 2×10^{-3} Hz also decrease with time (Figure 3d & h). Spectral slopes at these frequencies are observed to flatten (i.e. whiten). While longer periods contain less power at later experimental times, they continue to contribute significantly to the total power, shown by the spectral slope steepening as the system evolves in time. Pressure at shorter periods ($< 10^3$ s) contributes far less ($\sim 2\%$) to total power in both the oil/water and gas/water experiments.

When averaged over the entire experimental run time, as shown in Figure 3c and g, spectral power can be described by a single spectral slope of -2 i.e. red noise for both experiments. However, at the end of both experiments (the darkest green lines in Figure 3d and h) the time-averaged power requires two spectral slopes, and differ for gas/water and oil/water, with a steeper spectral slope for frequencies $> 10^{-3}$ Hz for the latter.

3.3.2 The Role of Heterogeneity

The role of heterogeneity is evident in Figures 3a-d and i-l. In the experiment where the section of the sample with a lower porosity was closest to the inlet, there is an overshoot in pressure prior to stabilisation (seen in Figure 3i) at approximately 200 s. Whereas, when flow direction is reversed, there is a gradual increase in pressure, and no marked overshoot, as shown in Figure 3a. Both experiments reach the same differential pressure of approximately 200 kPa within 15 minutes of injection.

For both experiments, pressure at lower frequencies decreases in power with time (shown in Figure 3d and l). Power is increasingly concentrated at lower frequencies during an experiment, regardless of the orientation of the sample. During steady-state flow, the spectral slope for higher frequencies ($< 10^{-3}$ Hz) resembles white noise i.e. the amplitude is independent of frequency, while it is steeper for the lower frequencies. The spectral slope is -2 (red noise) when averaged over the whole time series. However, the evolution of the flow properties is dependent on the heterogeneity of the pore space and its orientation with respect to flow. This means that previous heterogeneity classifications, that rely on average porosity and permeability values for the whole core, miss the importance of the orientation of heterogeneity with respect to the flow direction (Li & Benson, 2015; Ni et al., 2019).

3.4 Core-scale vs Pore-scale Results

The magnitude of pressure fluctuations are similar for the core-scale and pore-scale experiments (they are on the order of 1–5 kPa). The total pressure drop is significantly higher for the core-scale experiments, meaning the pressure fluctuations are much smaller relative to the total pressure drop across the sample.

While the magnitude of pressure fluctuations are similar, spectral analysis reveals differences between the pore-scale and core-scale experiments. First, the single spectral slope observed in the pore-scale oil/water experiment is not observed in the core-scale oil/water experiment. While the spectral slope is approximately -3 for frequencies $< 10^{-3}$ Hz during steady-state flow at the core-scale, it flattens to 0 (white noise), for the higher frequencies/shorter periods (Figure 3h). This suggests that the shorter periods are less significant in the core-scale experiments during steady-state flow. Secondly, at

periods 10^2 to 10^4 s, power increases in the pore-scale gas/water experiment, while the shorter periods (down to ~ 10 s) remain approximately constant (Figure 2d). For the core-scale gas/water experiments, power decreases across almost all periods (down to $\sim$ 10 s), albeit at a slower rate. Thus the evolution of the time-averaged power spectra is dependent on scale. While similar spectral slopes are observable (between -1 and -3), these slopes are dependent on frequency and time. In all cases, the shorter timescales play a more significant role during transient flow, but this significance decreases markedly for the core-scale experiments, possibly due to viscous dampening.

For the larger, core-scale experiments, a single spectral slope (attributed to the flow regime assumed in the multiphase extension of Darcy's law) is not observed under any of the experimental conditions explored in this work. This result suggests that the onset of non-linear flow may occur at lower capillary numbers in larger samples. This assertion agrees with dynamic pore network modelling observations showing that the onset of non-linear flow regimes start at lower flow rates as system size increases (Hansen et al., 2023; Pedersen & Hansen, 2023).

4 Conclusions

In this work we used continuous wavelet transformation to investigate sources of spectral power in the pressure time series of multiphase flow experiments. We showed that spectral power is dependent on frequency, sample size, and the heterogeneity present. Since pressure series spectral slopes are dependent on frequency and time, it is challenging to extrapolate flow dynamics to larger spatial scales and longer temporal scales in a straightforward way. However, we can relate spectral signals to dynamics in the pore space. This shows how pressure time series can provide useful information about the underlying pore-scale dynamics at larger scales. Thus, an analysis of the pressure fluctuations is an important step to understanding larger scale flow processes. We showed it is possible to gain new insights into the underlying flow regimes without recourse to novel experimental techniques, or increased imaging capabilities.

Further work is needed to fully characterize the impact of heterogeneity, e.g. layering or different lithologies, on spectral power and associated scaling regimes. Experiments should be conducted at lower flow rates, and different fractional flows to ascertain if the connected pathway flow signal observed for the pore-scale results is possible in core-scale experiments. Further work is also needed to create analytical spectra from physical models, to increase the applicability of the findings made in this work to other flow regimes and different samples.

5 Open Research

The pressure data shown in this work is attached in the Supporting Information.

The continuous wavelet transformation analysis is available on Github: `https://github.com/Malley1/Wavelets-pycwt-wrapper`.

References

Akin, S., & Kovscek, A. (2003). Computed tomography in petroleum engineering research. *Geological Society, London, Special Publications*, *215*(1), 23–38.

Avraam, D., & Payatakes, A. (1995). Flow regimes and relative permeabilities during steady-state two-phase flow in porous media. *Journal of Fluid Mechanics*, *293*, 207–236.

Bachu, S., & Adams, J. (2003). Sequestration of co2 in geological media in response to climate change: capacity of deep saline aquifers to sequester co2 in solution. *Energy Conversion and management*, *44*(20), 3151–3175.

Benson, S. M., Bennaceur, K., Cook, P., Davison, J., de Coninck, H., Farhat, K., ... others (2012). Carbon capture and storage. *Global energy assessment-Toward a sustainable future*, 993.

Berg, S., Ott, H., Klapp, S. A., Schwing, A., Neiteler, R., Brussee, N., ... others (2013). Real-time 3d imaging of haines jumps in porous media flow. *Proceedings of the National Academy of Sciences*, *110*(10), 3755–3759.

Blunt, M. J. (2017). *Multiphase flow in permeable media: A pore-scale perspective.* Cambridge University Press.

Boon, M., & Hajibeygi, H. (2022). Experimental characterization of h 2/water multiphase flow in heterogeneous sandstone rock at the core scale relevant for underground hydrogen storage (uhs). *Scientific Reports*, *12*(1), 14604.

Daley, T. M., Ajo-Franklin, J. B., & Doughty, C. (2011). Constraining the reservoir model of an injected co2 plume with crosswell cassm at the frio-ii brine pilot. *International Journal of Greenhouse Gas Control*, *5*(4), 1022–1030.

Dance, T., LaForce, T., Glubokovskikh, S., Ennis-King, J., & Pevzner, R. (2019). Illuminating the geology: Post-injection reservoir characterisation of the co2crc otway site. *International Journal of Greenhouse Gas Control*, *86*, 146–157.

Fernandes, V., Roberts, G., White, N., & Whittaker, A. (2022). North american landscape evolution: Insights from stratigraphy, thermochronology and geomorphology. *Authorea Preprints*.

Gao, Y., Lin, Q., Bijeljic, B., & Blunt, M. J. (2020). Pore-scale dynamics and the multiphase darcy law. *Physical Review Fluids*, *5*(1), 013801.

Hansen, A., Flekkøy, E. G., Sinha, S., & Slotte, P. A. (2023). A statistical mechanics framework for immiscible and incompressible two-phase flow in porous media. *Advances in Water Resources*, *171*, 104336.

Hosseini, S. A., Lashgari, H., Choi, J. W., Nicot, J.-P., Lu, J., & Hovorka, S. D. (2013). Static and dynamic reservoir modeling for geological co2 sequestration at cranfield, mississippi, usa. *International Journal of Greenhouse Gas Control*, *18*, 449–462.

Jackson, S. J., Agada, S., Reynolds, C. A., & Krevor, S. (2018). Characterizing drainage multiphase flow in heterogeneous sandstones. *Water Resources Research*, *54*(4), 3139–3161.

Jackson, S. J., & Krevor, S. (2020). Small-scale capillary heterogeneity linked to rapid plume migration during co 2 storage. *Geophysical Research Letters*, *47*(18), e2020GL088616.

Juanes, R., MacMinn, C. W., & Szulczewski, M. L. (2010). The footprint of the co 2 plume during carbon dioxide storage in saline aquifers: storage efficiency for capillary trapping at the basin scale. *Transport in porous media*, *82*(1), 19–30.

Krevor, S. C., Pini, R., Zuo, L., & Benson, S. M. (2012). Relative permeability and trapping of co2 and water in sandstone rocks at reservoir conditions. *Water resources research*, *48*(2).

Lenormand, R., Zarcone, C., & Sarr, A. (1983). Mechanisms of the displacement of one fluid by another in a network of capillary ducts. *Journal of Fluid Mechanics*, *135*, 337–353.

Li, B., & Benson, S. M. (2015). Influence of small-scale heterogeneity on upward co2 plume migration in storage aquifers. *Advances in water resources*, *83*, 389–404.

Liu, Y., San Liang, X., & Weisberg, R. H. (2007). Rectification of the bias in the wavelet power spectrum. *Journal of Atmospheric and Oceanic Technology*, *24*(12), 2093–2102.

McClure, J. E., Berg, S., & Armstrong, R. T. (2020). Capillary fluctuations in non-equilibrium systems. *arXiv preprint arXiv:2012.09139*.

Mendez-Diaz, S., Serrano-Garcia, J., Zenit, R., & Hernandez-Cordero, J. (2013). Power spectral distributions of pseudo-turbulent bubbly flows. *Physics of Fluids*, *25*(4), 043303.

Mercado, J. M., Gomez, D. C., Van Gils, D., Sun, C., & Lohse, D. (2010). On bubble clustering and energy spectra in pseudo-turbulence. *Journal of fluid mechanics*, *650*, 287–306.

Moebius, F., & Or, D. (2014). Pore scale dynamics underlying the motion of drainage fronts in porous media. *Water Resources Research*, *50*(11), 8441–8457.

Moura, M., Måløy, K. J., Flekkøy, E. G., & Toussaint, R. (2017). Verification of a dynamic scaling for the pair correlation function during the slow drainage of a porous medium. *Physical Review Letters*, *119*(15), 154503.

Muskat, M. (1938). The flow of homogeneous fluids through porous media. *Soil Science*, *46*(2), 169.

Ni, H., Boon, M., Garing, C., & Benson, S. M. (2019). Predicting co2 residual trapping ability based on experimental petrophysical properties for different sandstone types. *International Journal of Greenhouse Gas Control*, *86*, 158–176.

O'Malley, C. P. B., & Roberts, G. G. (2022). Wavelets-pycwt-wrapper v.0.1.1 (https://github.com/Malley1/Wavelets-pycwt-wrapper). *GitHub*. Retrieved from `https://github.com/Malley1/Wavelets-pycwt-wrapper` doi: 10.5281/zenodo.7357231

Pedersen, H., & Hansen, A. (2023). Parameterizations of immiscible two-phase flow in porous media. *Frontiers in Physics*, *11*, 116.

Perrin, J.-C., Krause, M., Kuo, C.-W., Miljkovic, L., Charoba, E., & Benson, S. M. (2009). Core-scale experimental study of relative permeability properties of co2 and brine in reservoir rocks. *Energy Procedia*, *1*(1), 3515–3522.

Pini, R., & Benson, S. M. (2013). Simultaneous determination of capillary pressure and relative permeability curves from core-flooding experiments with various fluid pairs. *Water Resources Research*, *49*(6), 3516–3530.

Pini, R., & Madonna, C. (2016). Moving across scales: a quantitative assessment of x-ray ct to measure the porosity of rocks. *Journal of Porous Materials*, *23*, 325–338.

Ringrose, P., & Bentley, M. (2016). *Reservoir model design.* Springer.

Ringrose, P., Mathieson, A., Wright, I., Selama, F., Hansen, O., Bissell, R., . . . Midgley, J. (2013). The in salah co2 storage project: lessons learned and knowledge transfer. *Energy Procedia*, *37*, 6226–6236.

Roberts, G. G., White, N., & Lodhia, B. H. (2019). The generation and scaling of longitudinal river profiles. *Journal of Geophysical Research: Earth Surface*, *124*(1), 137–153.

Roghair, I., Mercado, J. M., Annaland, M. V. S., Kuipers, H., Sun, C., & Lohse, D. (2011). Energy spectra and bubble velocity distributions in pseudo-turbulence: Numerical simulations vs. experiments. *International journal of multiphase flow*, *37*(9), 1093–1098.

Rubin, E., & De Coninck, H. (2005). Ipcc special report on carbon dioxide capture and storage. *UK: Cambridge University Press. TNO (2004): Cost Curves for CO2 Storage, Part*, *2*, 14.

Rücker, M., Berg, S., Armstrong, R., Georgiadis, A., Ott, H., Schwing, A., . . . others (2015). From connected pathway flow to ganglion dynamics. *Geophysical Research Letters*, *42*(10), 3888–3894.

Rücker, M., Georgiadis, A., Armstrong, R. T., Ott, H., Brussee, N., Van der Linde, H., . . . Berg, S. (2021). The origin of non-thermal fluctuations in multiphase flow in porous media. *Frontiers in Water*, *3*, 671399.

Rudnick, D. L., & Davis, R. E. (2003). Red noise and regime shifts. *Deep Sea Research Part I: Oceanographic Research Papers*, *50*(6), 691–699.

Ruprecht, C., Pini, R., Falta, R., Benson, S., & Murdoch, L. (2014). Hysteretic trapping and relative permeability of co2 in sandstone at reservoir conditions. *International Journal of Greenhouse Gas Control*, *27*, 15–27.

Schlüter, S., Berg, S., Li, T., Vogel, H., & Wildenschild, D. (2017). Time scales of relaxation dynamics during transient conditions in two-phase flow. *Water Resources Research*, *53*(6), 4709–4724.

Spurin, C., Bultreys, T., Bijeljic, B., Blunt, M. J., & Krevor, S. (2019a). Intermittent fluid connectivity during two-phase flow in a heterogeneous carbonate rock. *Physical Review E*, *100*(4), 043103.

Spurin, C., Bultreys, T., Bijeljic, B., Blunt, M. J., & Krevor, S. (2019b). Mechanisms controlling fluid breakup and reconnection during two-phase flow in porous media. *Physical Review E*, *100*(4), 043115.

Spurin, C., Bultreys, T., Rücker, M., Garfi, G., Schlepütz, C. M., Novak, V., . . . Krevor, S. (2020). Real-time imaging reveals distinct pore-scale dynamics during transient and equilibrium subsurface multiphase flow. *Water Resources Research*, *56*(12), e2020WR028287.

Spurin, C., Bultreys, T., Rücker, M., Garfi, G., Schlepütz, C. M., Novak, V., . . . Krevor, S. (2021). The development of intermittent multiphase fluid flow pathways through a porous rock. *Advances in Water Resources*, *150*, 103868.

Spurin, C., Rücker, M., Moura, M., Bultreys, T., Garfi, G., Berg, S., . . . Krevor, S. (2022). Red noise in steady-state multiphase flow in porous media. *Water Resources Research*, *58*(7), e2022WR031947.

Thiyagarajan, S. R., Emadi, H., Hussain, A., Patange, P., & Watson, M. (2022). A comprehensive review of the mechanisms and efficiency of underground hydrogen storage. *Journal of Energy Storage*, *51*, 104490.

Torrence, C., & Compo, G. P. (1998). A practical guide to wavelet analysis. *Bulletin of the American Meteorological society*, *79*(1), 61–78.

van der Schaaf, J., Schouten, J., Johnsson, F., & Van den Bleek, C. (2002). Non-intrusive determination of bubble and slug length scales in fluidized beds by decomposition of the power spectral density of pressure time series. *International Journal of Multiphase Flow*, *28*(5), 865–880.

Zhang, Y., Bijeljic, B., Gao, Y., Lin, Q., & Blunt, M. J. (2021). Quantification of nonlinear multiphase flow in porous media. *Geophysical Research Letters*, *48*(5), e2020GL090477.

Zhao, B., MacMinn, C. W., & Juanes, R. (2016). Wettability control on multiphase flow in patterned microfluidics. *Proceedings of the National Academy of Sciences*, *113*(37), 10251–10256.

Zou, S., Armstrong, R. T., Arns, J.-Y., Arns, C., & Hussain, F. (2018). Experimental and theoretical evidence for increased ganglion dynamics during fractional flow in mixed-wet porous media. *Water Resources Research*.